Chinese Chemical Letters 36 (2025) 109531

Contents lists available at ScienceDirect

Chinese Chemical Letters

journal homepage: www.elsevier.com/locate/cclet

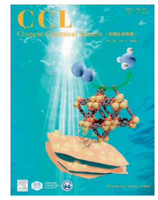

Stabilization of zinc anode by trace organic corrosion inhibitors for long lifespan

Wenfeng Shao[a,d,1], Chuanlin Li[a,1], Chenggang Wang[a], Guangsen Du[a], Shunshun Zhao[b], Guangmeng Qu[c], Yupeng Xing[d], Tianshuo Guo[d], Hongfei Li[d,*], Xijin Xu[a,*]

[a] School of Physics and Technology, University of Jinan, Ji'nan 250022, China
[b] State Key Laboratory of Chemical Resource Engineering, Beijing University of Chemical Technology, Beijing 100029, China
[c] School of Chemistry and Chemical Engineering, Shandong University, Ji'nan 250100, China
[d] School of System Design and Intelligent Manufacturing, Southern University of Science and Technology, Shenzhen 518000, China

ARTICLE INFO

Article history:
Received 23 November 2023
Revised 8 January 2024
Accepted 17 January 2024
Available online 19 January 2024

Keywords:
Solid electrolyte interface
Aqueous zinc-ion battery
Corrosion inhibitors
Electrolyte additive
Zinc anode

ABSTRACT

Aqueous zinc-ion batteries are highly favored for their enhanced safety and reduced cost. However, there exist challenges including zinc dendrite, hydrogen evolution, and surface corrosion to be solved. Using electrolyte additives is a highly convenient approach to solving zinc anode-related issues. Inspired by industrial corrosion protection, a trace amount of the corrosion inhibitor urotropine (URT) is used as an electrolyte additive to protect the zinc anode. Theoretical calculation and experimental analysis confirm the adsorption of URT molecules onto the surface of Zn, which inhibits hydrogen evolution. This adsorption further leads to the formation of an inorganic-organic bilayer solid electrolyte interface (SEI) on the surface of the zinc anode, effectively protecting the Zn anode from corrosion, hydrogen evolution and zinc dendrites. The presence of SEI enables symmetrical Zn//Zn cells to exhibit a long cycling performance of 1750 h at 1 mA/cm^2 and an average coulombic efficiency of 99.0% at 1 mA/cm^2 in Zn//Cu cells. After being coupled with polyaniline (PANI), the Zn//PANI full battery displays excellent cycle stability and specific capacity.

Aqueous zinc ion batteries (AZIBs) are widely regarded as a promising energy storage technology for their impressive theoretical capacity of 820 mAh/g, low potential of −0.76 V *versus* SHE and excellent safety profile [1,2]. There are also many specific applications of zinc ion batteries, such as zinc ion hybrid capacitors [3]. However, the occurrence of uneven deposition of zinc on the anode surface and the presence of aqueous electrolytes in aqueous systems result in unfavorable side reactions, which will lead to zinc dendrites, surface corrosion, and the hydrogen evolution reaction (HER) [4].

Currently, many strategies have been proposed to solve these issues, such as the use of new separators [5–7], electrolyte additives [8–10], the modification of Zn anodes [11,12], and the construction of protective layers [13–15]. In traditional lithium-ion batteries, researchers have also explored the design of electrode materials [16–18]. Among them, electrolyte additives are considered an effective approach due to their convenience and low cost [19]. Most reported work on electrolyte additives mainly focuses on preferentially adsorbing onto zinc metal surfaces, resulting in blocked contact between the zinc surface and H_2O [20]. By replacing H_2O in the Zn^{2+} solvated sheath to regulate the solvation structure of electrolytes [21], an *in-situ* solid electrolyte interface (SEI) is formed to facilitate ion transport and uniform Zn deposition [22,23]. In general, inorganic layers exhibit favorable ion conductivity but possess a notable rigidity. Conversely, organic layers offer enhanced flexibility. The fusion of organic and inorganic SEI layers can significantly improve the performance of zinc anodes and extend the lifespan of different zinc-ion batteries [24,25]. The solubility of general organic additives in water is limited, requiring the use of higher concentrations or expensive electrolytes, resulting in an increased cost [26]. Hence, the utilization of additives that effectively stabilize the SEI through trace addition emerges as the optimal selection.

Organic corrosion inhibitors have been widely used for corrosion protection as they can be adsorbed on metal surfaces through physical or chemical interactions to separate the metal surface from water [27]. Inspirationally, the metal corrosion in-

* Corresponding authors.
E-mail addresses: lihf@sustech.edu.cn (H. Li), sps_xuxj@ujn.edu.cn (X. Xu).
[1] These authors contributed equally to this work.

https://doi.org/10.1016/j.cclet.2024.109531

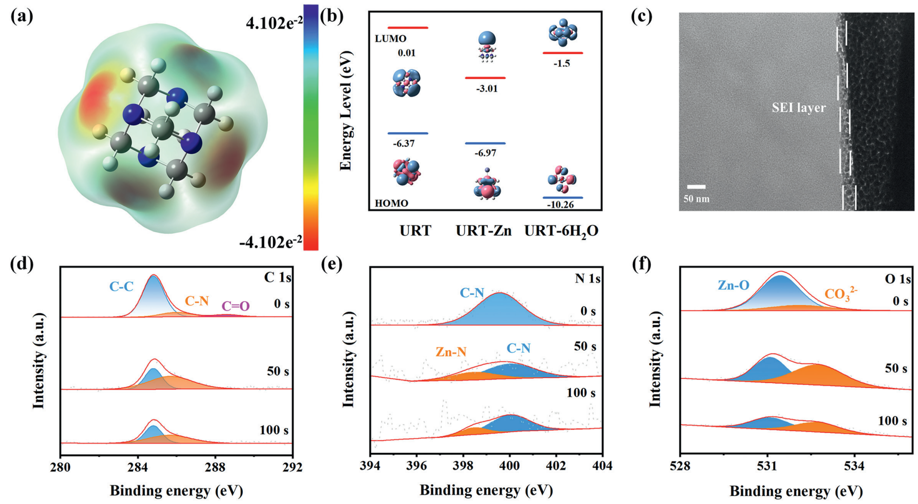

Fig. 1. (a) Electrostatic potential mapping of URT molecule. (b) The corresponding isosurface of the HOMO and LUMO levels with the free URT, the URT+ Zn and URT+ $6H_2O$ coordination. (c) TEM image and (d-f) XPS depth spectrum of Zn anode cycling 50 cycles in URT/$ZnSO_4$ electrolyte.

hibitor urotropine (URT) was used as an electrolyte additive and trace amounts (5 mmol/L) to the $ZnSO_4$ electrolyte to fully protect the zinc anode. Due to the adsorption of URT, the surface of the zinc anode avoids direct contact with water, thereby inhibiting corrosion and hydrogen evolution. The assembled Zn//Zn battery has excellent cycle life of 1750 h at 1 mA/cm^2 and the Zn//Cu battery has an average coulombic efficiency of up to 99.0% at 1 mA/cm^2 current density. Commercial polyaniline (PANI) is used as the cathode and the assembled Zn//PANI battery has excellent cycling performance (2000 cycles). This work provides a new strategy to improve the lifespan and stability of water-based zinc-ion batteries.

Two electrolytes of 1 mol/L $ZnSO_4$ solution and 1 mol/L $ZnSO_4$ with a 5 mmol/L URT additive are used. In addition, different quantities of URT at 1, 5, 20 mmol/L are added in $ZnSO_4$ electrolytes and the pH at various concentrations is conducted to study the influence of URT additive concentration on the electrolyte. Upon the addition of URT molecules at the concentrations of 1, 5, and 20 mmol/L to a solution of 1 mol/L $ZnSO_4$, the pH of the solution remains almost no change, only with very slight variation (5.57 to 5.58, 5.59, and 5.60 in Fig. S1 in Supporting information, respectively).

In addition to evaluating various electrolytes, contact angle measurements were performed to assess the wettability of the zinc anodes. The wettability of zinc anodes directly affects the uniform flow of zinc ions and guides uniform zinc ion electroplating [28]. In Fig. S2 (Supporting information), a contact angle of 89.1° can be observed on the surface of zinc foil in pure $ZnSO_4$ electrolyte. This is mainly due to its hydrophobicity, which resists the wetting behavior of electrolytes. In contrast, the contact angle of the $ZnSO_4$ electrolyte with the addition of additive URT shows a significant downward trend, with a measured contact angle of 72.8°, indicating that the modified electrolyte has enhanced wetting ability on the zinc surface and promotes the transport kinetics of zinc ions [29]. To screen for more suitable concentrations and understand the effect of URT electrolyte additives on the cycling stability of zinc ion batteries. When different concentrations of additives were added in and if the addition amount exceeded 20 mmol/L, the solution became cloudy and the additives could not be miscible with the solution (Fig. S3 in Supporting information). The cycling life of Zn//Zn symmetric batteries was compared with 1 mol/L $ZnSO_4$ electrolyte and URT additives containing 1, 5, 10 and 20 mmol/L concentrations at a current density of 1 mA/cm^2 and a capacity of 1 mAh/cm^2. In Fig. S4 (Supporting information), 1 mol/L $ZnSO_4$ electrolyte exhibited a cycle life of 140 h, followed by a short circuit. When 1 mmol/L URT additive is added, the cycle life increases to 262 h, and when the concentration of the additive is 5 mmol/L, the cycle life increases to 1750 h. But as the concentration of additives further increases to 20 mmol/L, the cycle life decreases. Therefore, URT additives have a certain promoting effect on the cycle life and stability of zinc, with a concentration of 5 mmol/L being the optimal.

From the electrostatic potential of URT molecules in Fig. 1a, the nitrogen atom possesses a more negative electrostatic potential, implying the strong interaction of electrostatic attraction between Zn^{2+} and URT molecules. The highest occupied molecular orbital (HOMO) and the lowest unoccupied molecular orbital (LUMO) of URT is conducted by the utilization of density functional theory. As presented in Fig. 1b, the LUMO energy level of URT is 0.01 eV. However, the energy levels reduce to −3.01 and −1.5 eV when in coordination with Zn and H_2O, respectively. Remarkably, the LUMO value of URT-Zn is lower than that of URT-H_2O, indicating that URT-H_2O is before trap electrons and is more likely reduced to form a SEI layer before H_2O. This *in situ* SEI effectively mitigates undesired side reactions on the surface of zinc.

X-ray photoelectron spectroscopy (XPS) and transmission electron microscopy (TEM) are employed to investigate the composition and structure of the SEI. The zinc is directly deposited onto the copper grid in the URT/$ZnSO_4$ electrolyte for TEM analysis. As a result, a distinct SEI layer on the zinc surface (Fig. 1c) is observed with an approximate thickness of 30 nm. Besides, the composition of the *in-situ* SEI is explored by XPS spectrum measurements with argon (Ar) ion etching. As shown in Fig. 1d, the peaks located at 284.5 eV and 286.4 eV in the C 1s spectrum corresponding to the functional groups of C–C and C–N, respectively (Fig. 1d), demonstrating the stable adsorption of URT molecules onto the anode surface during the discharge/charge process. After etching, the peak intensity attributed to the C–C bond decreases gradually, while the peak intensity associated with the C–N bond increases. This observation indicates that URT molecules have the potential to decompose and form organic SEI layers [30]. The presence of a C–N bond observed in the N 1s spectrum, as shown in Fig. 1e, provides additional evidence for the adsorption of the URT additive on the Zn surface. It is noted that the C–N bond is still observable in the N 1s spectrum even after etching and the Zn-N bond appears, which supports the conclusion that URT molecules decompose and contribute to the formation of an organic SEI layer on anode surface. Furthermore, the O1s spectrum in Fig. 1f exhibits the distinct peaks associated with $CO_3{}^{2-}$ and Zn-O at 532.2 eV and 531.4 eV.

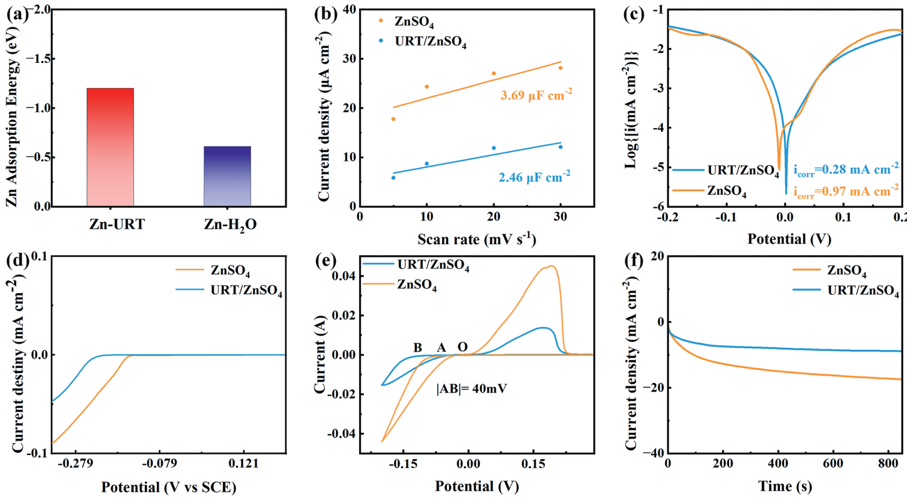

Fig. 2. (a) Comparison of adsorption energy of single Zn by URT and single Zn by H_2O. (b) Calculation of EDLC in pure $ZnSO_4$ and URT/$ZnSO_4$ electrolytes. (c) Tafel diagram of Zn metal tested at a scan rate of 5 mV/s in $ZnSO_4$ and URT/$ZnSO_4$ electrolytes. (d) LSV curves of Zn//Zn-symmetric batteries tested in pure $ZnSO_4$ and URT/$ZnSO_4$ electrolytes. (e) CV curves of Zn//Cu asymmetric batteries in pure $ZnSO_4$ and URT/$ZnSO_4$ electrolytes. (f) CA curves of pure $ZnSO_4$ and URT/$ZnSO_4$ electrolytes at a voltage of 0.15 V.

The peak intensity corresponding to CO_3^{2-} increased after etching at various depths, suggesting the presence of inorganic components within the SEI layer. XPS spectra of S 2p at different depths indicate that it is rich in inorganic ZnS layers (Fig. S5 in Supporting information). Consequently, the inorganic constituent of the resultant SEI primarily consists of ZnS and $ZnCO_3$. ZnS and $ZnCO_3$, confirm that SEI consists of an outer organic layer due to the decomposition of URT and an inner layer rich in inorganic ZnS and $ZnCO_3$. Based on the XPS data, it can be concluded that the SEI formed by URT/$ZnSO_4$ electrolyte exhibits an inorganic-organic bilayer structure, which consists of an internal inorganic layer composed of $ZnCO_3$ and ZnS and an external organic layer owing to the decomposition of URT. The existence of an organic-inorganic hybrid solid electrolyte interphase layer suggests a potential for high flexibility to accommodate volumetric changes, while simultaneously enabling fast Zn^{2+} transport.

The effect of URT additive on the solvation structure of Zn^{2+} was studied by attenuated total reflection Fourier transform infrared spectroscopy (ATR-FTIR) and Raman spectroscopy (Figs. S6 and S7 in Supporting information). There is no obvious deviation for the URT/$ZnSO_4$ electrolyte on the ATR-FTIR and Raman spectra, which is probably due to the trace amount of URT comparing to Zn^{2+} and the additive primarily functioning through interface adsorption. Thus, we calculated the adsorption energies of the additive URT molecule and H_2O with Zn, respectively. The binding energy of URT-Zn is −1.2 eV, which is much higher than the −0.61 eV of H_2O-Zn (Fig. 2a), indicating that the URT molecule is before adsorption onto the Zn surface. The URT additive will preferentially adsorb on the Zn metal anode and accumulate in an electric double layer (EDL) through strong electrostatic adsorption between negatively charged N atoms and positively charged site surfaces [31]. Consequently, the electric double layer capacitance (EDLC) for Zn anodes in $ZnSO_4$ electrolytes is measured to confirm it (Fig. 2b). Obviously, the EDLC of URT/$ZnSO_4$ electrolyte is 2.46 μF/cm^2, lower than pure $ZnSO_4$ electrolyte of 3.69 μF/cm^2. These results illustrate that the introduction of the URT additive positively influences the diffusion of Zn^{2+}. The EDS maps show a uniform distribution of Zn, S, O, and N elements (Fig. S8 in Supporting information), which are consistent with the composition of SEI. At the same time, the zeta potential test can also prove the adsorption of additive molecules. The Zeta potential in $ZnSO_4$ electrolytes is −0.86 mV, and the Zeta potential moves negatively to −6.47 mV after adding URT additive to it, but the potential is corrected compared with $ZnSO_4$ electrolytes, indicating that URT molecules are electronegative and can adsorb zinc ions (Fig. S9 in Supporting information). In addition, the TAFEL curves are tested to further demonstrate the corrosion inhibition effects of URT additives. As exhibited in Fig. 2c, the corrosion potential of Zn metal is increased from −0.013 V to 0.002 V (*vs.* Ag/AgCl) after introducing URT, and the corrosion current (i_{corr}) is reduced from 0.97 mA/cm^2 to 0.28 mA/cm^2, indicating that URT molecules significantly inhibit the corrosion reaction [32]. Besides, the overpotential of hydrogen evolution of URT/$ZnSO_4$ electrolyte is shifted to more negative (Fig. 2d) from the linear sweep voltammetry (LSV) test, manifesting that the URT additive greatly inhibits the hydrogen evolution. The by-products of alkaline zinc sulfate are further confirmed by X-ray diffraction (XRD) patterns at different current densities (Figs. S10 and S11 in Supporting information). It is observed that the URT additive dramatically inhibits the formation of by-products. Additionally, the R_{ct} (Fig. S12 in Supporting information) in EIS of URT/$ZnSO_4$ electrolyte is much smaller than pure $ZnSO_4$ electrolyte, which indicates that the URT additives greatly promote the charge transfer, in the consistency of the results of E_a. The nucleation overpotential of URT/$ZnSO_4$ electrolyte is 40 mV (|AB| = 40 mV) from the cyclic voltammetry (CV) curves with the scan rate of 10 mV/s in Fig. 2e, which promotes the nucleation kinetics of Zn [33]. The nucleation/growth behavior of URT/$ZnSO_4$ electrolyte is also detected by chronoamperometry (CA). As shown in Fig. 2f, the current density of the URT/$ZnSO_4$ electrolyte quickly increased in the first tens of seconds and then tended towards stability, implying rapidly realized a stable 3D diffusion utilizing the URT additives. In contrast, the current density of pure $ZnSO_4$ electrolytes is enlarged all the time, indicating a longer 2D diffusion process with a localized Zn deposition.

Scanning electron microscopy (SEM) was used to intuitively observe the influence of URT on the Zn plating/stripping. As displayed in Figs. 3a-c, the SEM image of the zinc anode is kept dense and smooth after cycling in the URT/$ZnSO_4$ electrolyte. In contrast, the surface (Fig. 3d) and the cross-section of zinc anode (Fig. S13 in Supporting information) in the $ZnSO_4$ electrolyte are suffused with Zn dendrite and by-products causing a rough surface. The *in-situ* optical microscope has recorded similar results. As displayed in Fig. 3e, the surface of the Zn anode in the URT/$ZnSO_4$ electrolyte exhibits a high degree of uniformity and smoothness from start to finish at a current density of 5 mA/cm^2. The reason for this phenomenon is that the URT molecules adsorb onto the surface of the Zn anode and decompose forming a SEI layer. And this SEI effectively promotes the uniform distribution of nucleation sites to inhibit the dendrite growth and induce uniform deposition of Zn

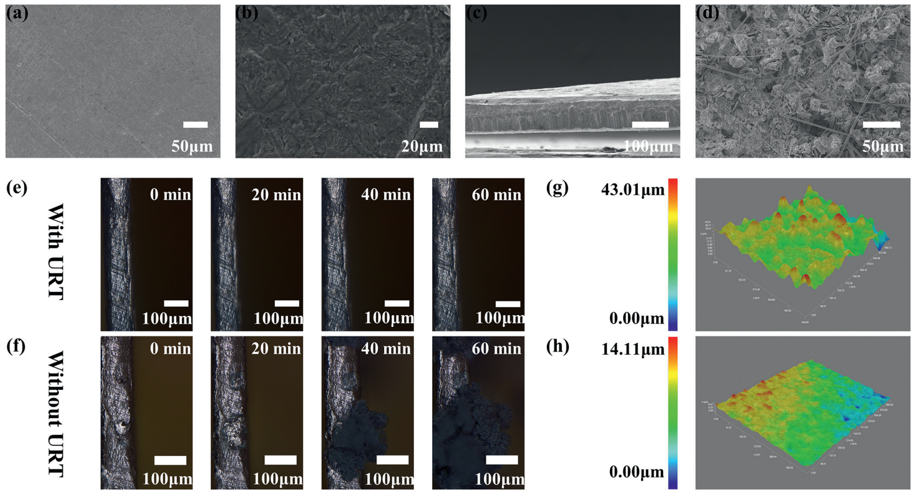

Fig. 3. SEM image of Zn surface cycled at 5 mA/cm^2 for 25 cycles in URT/$ZnSO_4$ electrolyte (a) at 50 µm standard, (b) at 20 µm standard, (c) cross-section of image. (d) SEM image of Zn surface cycled at 5 mA/cm^2 for 25 cycles in $ZnSO_4$ electrolyte. Optical microscope image of zinc deposition at 5 mA/cm^2 in (e) URT/$ZnSO_4$ electrolyte and (f) $ZnSO_4$ electrolyte. Ultra-depth three-dimensional microscopy image of Zn surface (g) cycled in $ZnSO_4$ electrolyte and (h) cycled in URT/$ZnSO_4$ electrolyte.

[34]. Nevertheless, in the case of pure $ZnSO_4$ electrolyte (Fig. 3f), the Zn dendrite emerges after a constant charge of 20 min. It is rapidly extended with further charge, which almost fills the whole space after charge to 60 min. This result further demonstrates the effectiveness of the URT decomposition into SEI for inhibiting dendrite growth. Additionally, the 3D morphological image obtained from ultra-depth three-dimensional microscopy (UTM) is obvious in height difference on the zinc anode in pure $ZnSO_4$ electrolyte after charging 5 mA/cm^2 (Fig. 3g). However, the surface morphology of Zn anode in URT/$ZnSO_4$ electrolyte is uniform (Fig. 3h). Atomic Force Microscope (AFM) images can demonstrate that the surface roughness of the zinc anode after cycling is correspondingly reduced after the addition of additive molecules (Fig. S14 in Supporting information). This observation provides additional evidence that the presence of URT molecules in the electrolyte contributes to the formation of a remarkably smooth Zn deposition morphology.

The DFT calculations and experimental analysis indicate that the URT additive in the $ZnSO_4$ electrolyte is before adsorb onto the surface of the zinc anode. Then the URT forms an SEI. This SEI layer serves to protect the zinc anode surface away from dendrite growth, hydrogen evolution, and by-products. Therefore, it is predictable that the Zn battery, in URT/$ZnSO_4$ electrolyte, exhibits remarkable cycle stability at various current densities. As shown in Fig. 4a, the long cycling life of the Zn//Zn symmetric battery in the URT/$ZnSO_4$ electrolyte could reach more than 1750 h at a cur-

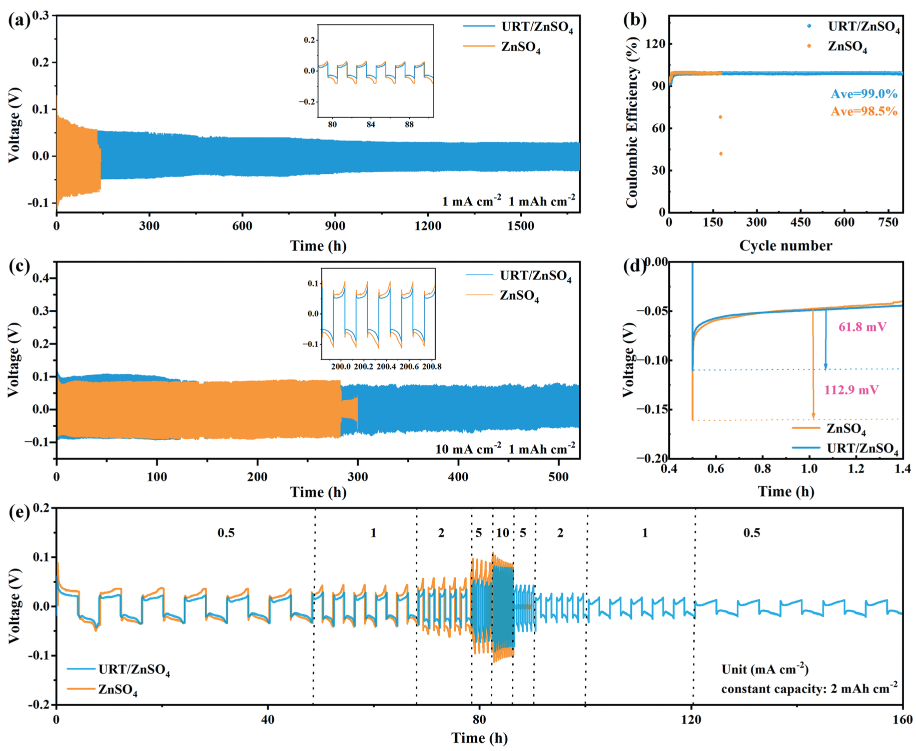

Fig. 4. (a) Long-term cycle performance of a Zn//Zn symmetric battery at 1 mA/cm^2 for 1 mAh/cm^2. (b) Coulombic efficiency of a Zn//Cu asymmetric battery at 1 mA/cm^2. (c) Long-term cycle performance of Zn//Zn symmetric batteries at 10 mA/cm^2 for 1 mAh/cm^2. (d) Nucleation overpotential of Zn anode in URT/$ZnSO_4$ and $ZnSO_4$ electrolyte at 5 mA/cm^2. (e) Rate performance of a Zn//Zn symmetric battery with $ZnSO_4$ electrolyte and URT/$ZnSO_4$ electrolyte.

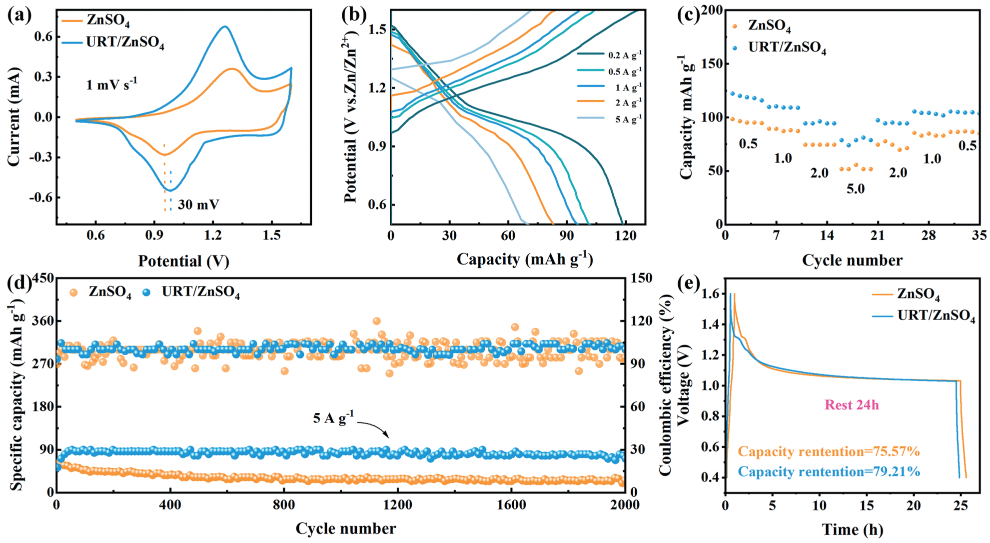

Fig. 5. (a) CV curves for Zn//PANI full battery in different electrolytes. (b) Charge/discharge curves at different current densities. (c) Rate performance at different current densities (Unit: A/g). (d) Long-term cycling performance at 5 A/g after 2000 cycles. (e) Self-discharge curves.

rent density of 1 mA/cm^2 with a deposition capacity of 1 mAh/cm^2. Besides, the Zn//Cu battery demonstrated a substantial increase in its cycle life, reaching a remarkable 800 cycles, where the battery exhibited a higher coulombic efficiency of 99.0% with a deposition capacity of 0.5 mAh/cm^2 (Fig. 4b). In comparison, the long cycling life of pure $ZnSO_4$ electrolytes only survived 177 cycles with a lower Coulombic efficiency of 98.5%. The Zn//Zn symmetric battery exhibits the sizable cycle life of 10 mA/cm^2 (Fig. 4c). These results are mainly due to that the URT adsorb onto the Zn anode inducing the Zn^{2+} uniform deposition without dendrite and parasitic side reactions, which greatly prolong the long cycling life.

Furthermore, as depicted in Figs. S15 and S16 (Supporting information), the Zn//Cu half-cell in the URT/$ZnSO_4$ electrolyte exhibits a lower overpotential of approximately 35 mV, which is mainly due to that the absorbed URT on the surface promotes the Zn^{2+} transfer in consistence with the results of lower E_a. As shown in Fig. 4d, the nucleation overpotential of the URT/$ZnSO_4$ electrolyte is 61.8 mV, while the nucleation overpotential of pure $ZnSO_4$ is up to 112.9 mV. This suggests that the presence of URT molecules facilitates the efficient transfer of $Zn^{2+}$from the interface between the anode and the electrolyte. And this result is also confirmed by the rate performance. As depicted in Fig. 4e, the battery in URT/$ZnSO_4$ electrolyte was charged/discharged from 0.5 mA/cm^2 to 10 mA/cm^2, and the shapes of charged/discharged curves were well kept with only the overpotential slightly increased. And well back to the initial state after the rate cycle. In contrast, the battery in pure $ZnSO_4$ electrolyte died in a short circuit after a high rate of charge/discharge. All these results provide robust evidence that the URT effectively protects the Zn anode away from dendrite growth, hydrogen evolution and by-products. This approach significantly enhanced reversibility in terms of Zn plating/stripping processes and enabled the battery to exhibit prolonged cycling capabilities.

To investigate the practical applicability of this URT/$ZnSO_4$ electrolyte, a Zn//PANI full battery was fabricated using commercial polyaniline (PANI). As displayed in Fig. 5a, the CV curves in URT/$ZnSO_4$ electrolyte at different scan rates exhibit a pair of redox peaks well in agreement with the results in pure $ZnSO_4$ electrolyte, revealing that the URT does not affect the redox reaction of the cathode. Furthermore, the CV curve of URT/$ZnSO_4$ electrolyte has a smaller voltage polarization (30 mV) compared to pure $ZnSO_4$ electrolyte, indicating that the reversibility of Zn//PANI full battery is improved after the addition of electrolyte additives. A similar result is also observed in galvanostatic charge and discharge (GCD) curves of Zn//PANI batteries at various current densities (Fig. 5b and Fig. S17 in Supporting information). The Nyquist curves in Fig. S18 (Supporting information) show a smaller semicircle in the high-frequency region corresponding to a smaller charge-transfer resistance, which enables faster ion transport for Zn plating/stripping. Fig. 5c illustrates the rate performance of Zn//PANI batteries at various current densities. The introduction of URT additive molecules to the $ZnSO_4$ electrolyte leads to an obvious enhancement in the capacity performance of Zn//PANI batteries across different current densities. This result indicates that the SEI generated through the decomposition of URT additive molecules significantly enhances the long-term durability of the zinc electrode and enhances the electrochemical performance of the complete battery system. Moreover, the Zn//PANI battery in the URT/$ZnSO_4$ electrolyte possesses long-term cycling stability (Fig. 5d), which exhibits a remarkable capacity of 80.2 mAh/g after 2000 cycles at 5 A/g. In contrast, the capacity in pure $ZnSO_4$ electrolyte is only 31.2 mAh/g. Furthermore, the self-discharge behavior is monitored to assess the effect of URT in mitigated side reaction during battery storage (Fig. 5e). After charging to 1.6 V, the battery is allowed to rest for 24 h and then discharged to 0.4 V. The Zn//PANI battery in URT/$ZnSO_4$ electrolyte has 79.21% capacity retention, higher than the 75.57% in pure $ZnSO_4$ electrolyte.

In summary, a trace amount of metal corrosion inhibitor URT was treated as an electrolyte additive to protect the Zn anode. It is found that the added URT molecules preferentially adsorbed on the Zn surface, enabling uniform deposition of Zn^{2+}on the recycled Zn surface. The inorganic-organic bilayer SEI layer formed *in situ* can suppress HER and Zn anode corrosion. Due to the role of SEI, the assembled Zn//Zn battery has excellent cycle life at 1 mA/cm^2 and a high average coulombic efficiency of 99.0% at a current density of 1 mA/cm^2. The assembled Zn//PANI battery has excellent cycling performance (2000 cycles). This work provides a method to improve the lifespan and stability of AZIBs.

Declaration of competing interest

We declare that we do not have any commercial or associative interest that represents a conflict of interest in connection with the work submitted.

Acknowledgments

The work was financially supported by Joint Funds of the National Natural Science Foundation of China (No. U22A20140), the National Natural Science Foundation of China (No. 22379062). This work was also supported by Shenzhen Stable Support Plan Program for Higher Education Institutions Research Program (No. 20220816131408001) and Shenzhen Science and Technology Program (No. JCYJ20230807091802006).

Supplementary materials

Supplementary material associated with this article can be found, in the online version, at doi:10.1016/j.cclet.2024.109531.

References

[1] Z. Cao, H. Zhang, B. Song, et al., Adv. Funct. Mater. 33 (2023) 2300339.
[2] Z. Hu, Z. Song, Z. Huang, et al., Angew. Chem. Int. Ed. 38 (2023) e202309601.
[3] J. Yao, F. Li, R. Zhou, et al., Chin. Chem. Lett. 35 (2024) 108354.
[4] C. Li, G. Qu, X. Zhang, et al., Energy Environ. Mater. 7 (2023) e12608.
[5] Y. Song, P. Ruan, C. Mao, et al., Nano-Micro Lett. 14 (2022) 218.
[6] Y. Liu, S. Liu, X. Xie, et al., J. InfoMat 5 (2023) e12374.
[7] Y. Fang, X. Xie, B. Zhang, et al., Adv. Funct. Mater. 32 (2022) 2109671.
[8] Y. Liu, Q. Shi, Y. Wu, et al., Chem. Eng. J. 407 (2021) 127189.
[9] M. Qiu, P. Sun, A. Qin, G. Cui, W. Mai, Energy Storage Mater 49 (2022) 463–470.
[10] D. Yuan, J. Zhao, H. Ren, et al., Angew. Chem. 133 (2021) 7289–7295.
[11] Z. Shen, L. Luo, C. Li, et al., Adv. Energy Mater. 11 (2021) 2100214.
[12] K. Qi, W. Zhu, X. Zhang, et al., ACS Nano 16 (2022) 9461–9471.
[13] X. Zhang, C. Li, G. Qu, et al., Smart Mat 5 (2024) e1212.
[14] Z. Zhao, R. Wang, C. Peng, et al., Nat. Commun. 12 (2021) 6606.
[15] H. Yang, Z. Chang, Y. Qiao, et al., Angew. Chem. 132 (2020) 9463–9467.
[16] X. Yin, L. Zhu, Y. Zhang, et al., Electrochim. Acta 469 (2023) 143226.
[17] G. Shen, B. Li, Y. Xu, et al., J. Colloid Interface Sci. 653 (2024) 1588–1599.
[18] L. Zhu, G. Ding, Q. Han, et al., Rare Metals 41 (2022) 25–437.
[19] J. Wan, R. Wang, Z. Liu, et al., ACS Nano 17 (2023) 1610–1621.
[20] S.J. Zhang, J. Hao, D. Luo, et al., Adv. Energy Mater. 11 (2021) 2102010.
[21] X. Lin, G. Zhou, M.J. Robson, et al., Adv. Funct. Mater. 32 (2022) 2109322.
[22] H. Liu, J.G. Wang, W. Hua, et al., Energy Environ. Sci. 15 (2022) 1872–1881.
[23] H.J. Kim, S. Kim, K. Heo, et al., Adv. Energy Mater. 13 (2023) 2203189.
[24] G. Ma, L. Miao, Y. Dong, et al., Energy Storage Mater 47 (2022) 203–210.
[25] D. Xie, Y. Sang, D.H. Wang, et al., Angew. Chem. Int. Ed. 62 (2023) e202216934.
[26] H. Yu, D. Chen, T. Zhang, et al., J. Small Struct. 3 (2022) 2200143.
[27] Z. Liu, J. Ren, F. Wang, et al., ACS Appl. Mater. Interfaces 13 (2021) 27085–27095.
[28] C. Meng, W. He, Z. Kong, et al., Chem. Eng. J. 450 (2022) 138265.
[29] P. Wang, S. Liang, C. Chen, et al., Adv. Mater. 34 (2022) 2202733.
[30] D. Li, L. Cao, T. Deng, et al., Angew. Chem. Int. Ed. 60 (2021) 13035–13041.
[31] H. Yu, D. Chen, X. Ni, et al., Energy Environ. Sci. 16 (2023) 2684–2695.
[32] X. Xie, S. Liang, J. Gao, et al., Energy Environ. Sci. 13 (2020) 503–510.
[33] D. Han, Z. Wang, H. Lu, et al., Adv. Energy Mater. 12 (2022) 2102982.
[34] K. Wang, T. Qiu, L. Lin, et al., Energy Storage Mater 54 (2023) 366–373.